

Numerical simulation using cellular Potts model for wound closure with ATP release and the mechanobiological effects

Kenta Odagiri ^{1,2} , Hiroshi Fujisaki ^{2,3} , Hiroya Takada ^{2,4,5} and Rei Ogawa ^{2,5}

¹ School of Network and Information, Senshu University, 2-1-1, Higashi-Mita, Tama, Kawasaki, Kanagawa 214-8580, Japan; k-oda@isc.senshu-u.ac.jp

² AMED-CREST, Japan Agency for Medical Research and Development, 1-1-5 Sendagi, Bunkyo-ku, Tokyo 113-8603, Japan

³ Department of Physics, Nippon Medical School, 1-7-1 Kyonan-cho, Musashino, Tokyo 180-0023, Japan; fujisaki@nms.ac.jp

⁴ Department of Anti-Aging and Preventive Medicine, Nippon Medical School, 1-1-5 Sendagi, Bunkyo-ku, Tokyo 113-8603, Japan; h-takada@nms.ac.jp

⁵ Department of Plastic, Reconstructive and Aesthetic Surgery, Nippon Medical School, 1-1-5 Sendagi, Bunkyo-ku, Tokyo 113-8603, Japan; r.ogawa@nms.ac.jp

* Correspondence: k-oda@isc.senshu-u.ac.jp; Tel: +81-44-900-7915

Abstract: To computationally investigate the recent experimental finding such that extracellular ATP release caused by exogenous mechanical forces promote wound closure, we introduce a mathematical model, the Cellular Potts Model (CPM), which is a popular discretized model on a lattice, where the movement of a "cell" is determined by a Monte Carlo procedure. In the experiment, it was observed that there is mechanosensitive ATP release from the leading cells facing the wound gap and the subsequent intracellular Ca^{2+} influx. To model these phenomena, the Reaction-Diffusion equations for ATP and Ca^{2+} concentrations are adopted and combined with CPM, where we also add a polarity term because the cell migration is enhanced in the case of ATP release. From the numerical simulations using this hybrid model, we discuss effects of the collective cell migration due to the ATP release and the Ca^{2+} influx caused by the mechanical forces and the consequent promotion of wound closure.

Keywords: Cellular Potts Model; Reaction-diffusion equations; Wound closure; Mechanobiology; Collective cell migration; contact inhibition

1. Introduction

Recent studies in the field of mechanobiology [1–3] have revealed that cells recognize and respond to various external stimuli or external forces, and it has been found that various biological functions in vivo are triggered by this mechanobiological effects [4–9]. As such, mechanobiological issues are important and challenging not only for basic biology but also for the optimal treatment of plastic surgery which is called "mechanotherapy" [10–14].

In relation to wound closure and mechanobiology, Takada, Furuya and Sokabe found that the mechanical forces on cells are important for wound closure [15]. In their experiment, a linear wound was made in cultured vascular endothelial cells, and the wound closure process was examined by applying stretch stimulation. It was found that the wound closure rate increased with the stretch stimulation compared to no external stimulation. They also measured real-time imaging of ATP and Ca^{2+} concentrations, where the stretch stimulation releases large amounts of ATP from the cells closest to the wound gap. Here ATP functions as an extracellular messenger and increases intracellular Ca^{2+} levels. When ATP travels like a transient wave from the proximal wound to the posterior cell, it is followed by a transient wave of Ca^{2+} . It was shown that the response of the cells to Ca^{2+} was indispensable for the wound closure because the Ca^{2+} wave disappeared and cell migration did not occur when the extracellular Ca^{2+} was removed.



Citation: Odagiri, K.; Fujisaki, H.; Takada, H.; Ogawa, R. Title. *Preprints* 2022, 1, 0. <https://doi.org/>

Publisher's Note: MDPI stays neutral with regard to jurisdictional claims in published maps and institutional affiliations.



Copyright: © 2022 by the authors. Licensee MDPI, Basel, Switzerland. This article is an open access article distributed under the terms and conditions of the Creative Commons Attribution (CC BY) license (<https://creativecommons.org/licenses/by/4.0/>).

Motivated by this experimental study, we here propose a mathematical model of wound closure process that explicitly considers ATP release by mechanical stimulation to the cells, the accompanying change in Ca^{2+} concentration, and collective cell migration by response to Ca^{2+} . We construct a hybrid model of the Cellular Potts Model (CPM) [16–22] and the Reaction-Diffusion (RD) equations [23,24], where CPM represents the dynamics of cells, such as cell migration and cell growth, and RD represents the changes in ATP and Ca^{2+} concentration. The cell migration in response to Ca^{2+} is expressed as self-propulsion driven by cell polarity, which is further added as an energy term in the CPM. Using this hybrid model, we try to numerically simulate the experiment on wound closure by Takada and coworkers.

This paper is organized as follows. In Sec. II, we first introduce the hybrid mathematical model for the wound closure process. We next show the numerical results of our model in Sec. III. To compare with the experimental results such that the wound closure is promoted by applying the mechanical stimulation, we here examine two different scenarios with and without ATP release. We also discuss why the wound closure rates are different in these two cases. Finally, we conclude this paper in Sec. IV.

2. Computational Model

We here introduce a mathematical model of cellular dynamics for wound closure, taking into account the intracellular ATP release and the subsequent extracellular Ca^{2+} influx by the mechanical stimulation. To couple the cellular dynamics with the spatio-temporal dynamics of the chemical components inside and outside of the cells, we propose a hybrid model of the Cellular Potts Model and the Reaction-Diffusion Equations. The former model represents the cellular population dynamics and the latter represents the spatio-temporal dynamics of ATP and Ca^{2+} , and the details are explained below.

2.1. Cellular Dynamics

Collective cell migration is one of the key processes in the wound closure process, and various mathematical models have been proposed [25–29]. We here employ the Cellular Potts Model (CPM) for the computational modeling of the cellular collective movement. CPM is defined on a lattice, representing a cell shape as a group of sites on the lattice. Each site has a cell index σ , where the same cell shares the same cell index σ . To mimic various cellular behavior such as cell deformation and migration, CPM repeats the "exchange" of adjacent lattice sites with a Metropolis algorithm using a kind of "energy" as described below.

The move is described as an attempt to copy the cell index $\sigma(\vec{x})$ at a randomly selected site \vec{x} into another randomly selected neighboring site \vec{x}' . Whether the move is accepted or not is determined using the change in the total energy ΔE due to the exchange. When $\Delta E \leq 0$, the move is always accepted, however, when $\Delta E > 0$, the move is accepted with the following probability: $p(\vec{x} \rightarrow \vec{x}') = \exp(-\beta\Delta E)$ where β denotes the magnitude of cell fluctuation, in accord with the conventional Metropolis algorithm.

2.2. Energy of Cell Population

The energy of cell population used in the CPM calculations is modelled as follows:

$$E_{\text{CPM}} = \sum_{\vec{x}, \vec{x}'} J_{\tau(\sigma(\vec{x})), \tau(\sigma(\vec{x}'))} \left(1 - \delta_{\sigma(\vec{x}), \sigma(\vec{x}')} \right) + \sum_k \lambda_V (V_k - V_{t,k})^2 + \sum_k \lambda_S (S_k - S_{t,k})^2 - E_{\text{mig}}, \quad (1)$$

where the first term represents the interfacial energy due to the cell adhesion, \vec{x} and \vec{x}' denote two neighboring lattice sites, $\sigma(\vec{x})$ denotes a cell index at a lattice site \vec{x} , and τ denotes a cell

type. (Note that the cell index refers to a single cell, whereas the cell type does bunches of cells.) $J_{\tau,\tau'}$ denotes the adhesion energy between cell type τ and τ' . The second term represents cell volume constraint energy, where V_k and $V_{t,k}$ denote a calculated volume and a target volume of cell k , respectively, and λ_V is the strength of the volume constraint. The third term represents cell surface constraint energy, where S_k and $S_{t,k}$ denote a calculated surface and a target surface of cell k , respectively, and λ_S is the strength of the surface constraint. (In two-dimensional system, cell surface area means the length of cell's perimeter.) The last term represents a cell migration energy due to cellular self-propulsion as described below.

2.3. Cellular Self-Propulsion

The cell migration energy E_{mig} with the self-propulsion is given by

$$E_{\text{mig}} = \sum_k P \frac{\vec{p}_k}{|\vec{p}_k|} \cdot \vec{v}_k, \quad (2)$$

where \vec{p}_k represents the cell polarity vector of cell k and \vec{v}_k represents the displacement vector of the center of cell k due to the Monte Carlo move. P is the strength of the cell autonomous motility. This formulation indicates that the cell polarity, which reflects the spatial differences in the biochemical state of a cell, drives cellular self-propulsion. Szabó and Cziráok proposed that the cell polarity vector \vec{p}_k decays spontaneously but reinforced by cell displacements [30,31]. We here assume that Ca^{2+} ions enhance the cellular self-propulsion and therefore the cell polarity vector is also reinforced in proportion to the amount of Ca^{2+} . In each Monte Carlo step (MCS), the change in \vec{p}_k is thus given by

$$\Delta \vec{p}_k = -\gamma \vec{p}_k + \Delta \vec{g}_k + \lambda_c \sum_{\vec{x}_k} W(C(\vec{x}_k)) (\vec{x}_k - \vec{g}_k). \quad (3)$$

The first term indicates spontaneous decay of \vec{p}_k with decay rate γ . The second term indicates reinforcement of \vec{p}_k resulting from cell displacements, where \vec{g}_k and $\Delta \vec{g}_k$ are the center of cell k and the change in \vec{g}_k during the MCS. The last term indicates reinforcement of the cell polarity due to intracellular Ca^{2+} ions, where $C(\vec{x})$ is the concentration of Ca^{2+} ion at position \vec{x} in cell k , $W(C(\vec{x}_k)) = \exp\left(-\frac{1}{wC(\vec{x})}\right)$ is the weight function of $C(\vec{x}_k)$, w is the weight coefficient of $C(\vec{x}_k)$, and λ_c is the magnitude of Ca^{2+} ion's enhancement of \vec{p}_k .

2.4. Dynamics of Chemical Components

The change in the concentration of extracellular ATP $A(\vec{x}, t)$ and intracellular Ca^{2+} $C(\vec{x}, t)$ are modelled by the following Reaction-Diffusion equations.

$$\frac{\partial A(\vec{x}, t)}{\partial t} = \delta_{\sigma(\vec{x}), \sigma_{\text{Edge}}} \theta(t) \theta(t_b - t) k_0 - \delta_{\sigma(\vec{x}), \sigma_{\text{cells}}} k_A A(\vec{x}, t) + D_C \nabla^2 A(\vec{x}, t), \quad (4)$$

$$\frac{dC(\vec{x}, t)}{dt} = \delta_{\sigma(\vec{x}), \sigma_{\text{cells}}} \theta(A_{\text{th}}) k_C (C_0 - C(\vec{x}, t)). \quad (5)$$

The first and second terms on the right hand side of Equation (4) denote ATP release and ATP consumption. ATP molecules release from only the leading cells σ_{Edge} that faces the wound edge at the beginning of the cell migration ($0 \leq t \leq t_b$) and are consumed by cells σ_{cells} with rate k_A as indicated by the second term. $\theta(t)$ is the Heaviside function (1 when $t > 0$ and 0 otherwise), t_b is the time when the ATP release ends, and k_0 is the release rate of ATP. The last term in Eq. (4) denotes the extracellular diffusion of ATP with the diffusion coefficient D_C . Equation (5) represents the intracellular Ca^{2+} response in the cells σ_{cells} induced by released extracellular ATP molecules, where A_{th} is the threshold value of the ATP concentration for the

extracellular Ca^{2+} influx due to the Ca^{2+} response, k_C is the influx rate of Ca^{2+} , and C_0 is the steady-state concentration of extracellular Ca^{2+} .

2.5. Cell Growth and Contact Inhibition

We further introduce the cell growth considering the contact inhibition. Contact inhibition is the mechanism which normal cells stop proliferation or growth when they contact each other.

Cell growth is modelled by increasing the target volume $V_{t,k}$ and the target surface area $S_{t,k}$ [32,33] in the CPM. When the cell k is not completely surrounded by other cells, the values of $V_{t,k}$ and $S_{t,k}$ increase in a cycle P_C , where the maximum sizes are V_{\max} and S_{\max} , respectively. On the other hand, when the cell is completely surrounded by the other cells, the values of $V_{t,k}$ and $S_{t,k}$ does not change, that is, the cell does not get large due to the effect of the contact inhibition.

Incidentally, we do not consider the cell division in this model, because the time scale of the experimental results [15] is shorter than that of the cell division (a cell does not divide within the simulation time).

3. Results and Discussion

We here show some numerical results using the hybrid model (CPM with polarity + RD equations for chemicals + contact inhibition for cells) for the wound closure process. To mimic the experimental situation [15], we set up the initial distribution of cells as shown in Fig 1 (a). The gap region (grey) between the upper and lower cells represents the linear wound. Green cells in Fig 1 (a) indicates the leading cells that face the wound edge. Only these leading cells release ATP molecules, as in the experiment [15], at the beginning of the simulation (cell migration) until $t_b = 1$. The initial volume of each cell is 25 (5×5) units, where we consider a square lattice with 1×1 unit, and the initial number of the cells is 288. (The total system size is 120×120 units and the wound region is the half of it.) Table 1 shows the parameters of the numerical simulation (units are arbitrary). J_{CC} and J_{CM} denote the cell-cell adhesion energy and the cell-medium (cell free area) adhesion energy, respectively.

To clarify the effect of the collective cell migration due to the ATP release and the subsequent Ca^{2+} influx resulting from the mechanical forces, we here numerically examine two different scenarios with and without the ATP release: The former is referred to as ATP model and the latter as ATP-free model. Compared to our previous study of the wound closure [34], we add to this model the effect of contact inhibition and investigate in detail the effects of the ATP release. This makes the this study more suitable for comparison with the previous experimental study [15].

Table 1. Parameters used in the simulations (arbitrary units).

J_{CC}	9.0	J_{CM}	3.0	λ_V	2.0	λ_S	0.5	λ_c	5.0	P	2.0
γ	0.025	w	10.0	k_0	10.0	k_A	0.01	D_C	0.1	A_{th}	0.1
k_C	1.0	C_0	1.0	P_C	10	V_{\max}	60	S_{\max}	38.7		

3.1. Wound closure by the collective cell migration

Figure 1 (b) and (c) show the time evolution of the wound closure process in the ATP-free model and ATP model, respectively. These figures clearly show that the wound gap closes more quickly in the ATP model than in the ATP-free model. In the ATP model, the cells facing the wound gap rapidly migrate forward, and this quick migration causes rapid closure of the wound gap. On the other hand, in the ATP-free model, the leading cells migrate forward very slowly, and thus the wound gap closes very slowly.

To compare the rate of wound closure in these models, we measure the change in the surface coverage by cells over time (Fig. 2). Although the rate of wound closure in the two cases is almost the same at the early phase ($t = 0 \sim 200$), the rate in the ATP-free model suddenly slows down after around $t=400$. On the other hand, in the ATP model, the wound closure rate does not slow down significantly until cells fill most of the wound gap. Therefore, the ATP release clearly shows the promotion of the wound closure with the parameters we chose in Table 1.

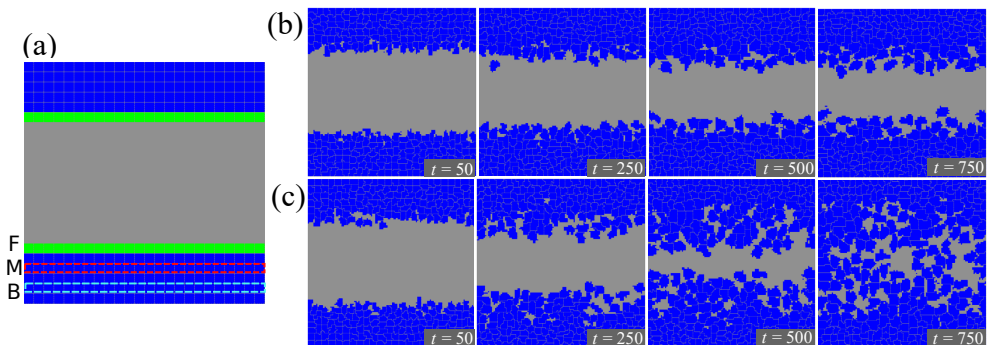


Figure 1. (a) Initial distribution of cells. F, M and B represent cells facing the wound gap, cells located in the middle of the cell cluster and cells located at the back of the cell cluster, respectively. (b) and (c) Time evolution of wound closure process in the ATP-free model and the ATP model, respectively.

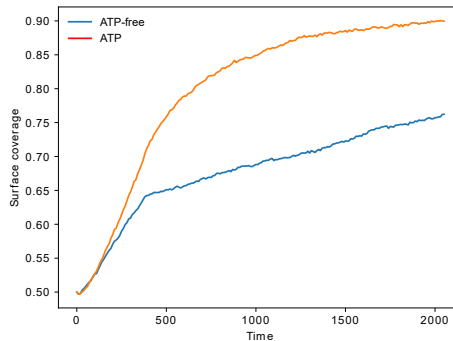


Figure 2. Time evolution of the surface coverage by cells in the ATP-free model and the ATP model.

3.2. ATP diffusion and Ca^{2+} response

We next show the ATP diffusion and the subsequent Ca^{2+} response at the early stage in the ATP model. In the previous experimental study [15], the diffusion of released ATP and the subsequent Ca^{2+} response have been observed within a few seconds after mechanical stimulation. Figure 3 (a), (b) and (c) show the time evolution of the distribution of cells, ATP and Ca^{2+} at the early stage, respectively. The released ATP from the leading cells diffuses quickly and the resulting Ca^{2+} influx occurs although the width of the wound gap is almost the same ($t = 10 \sim 50$). And after a while, the diffused ATP decays ($t = 100, 250$). These results qualitatively correspond to the experimental results.

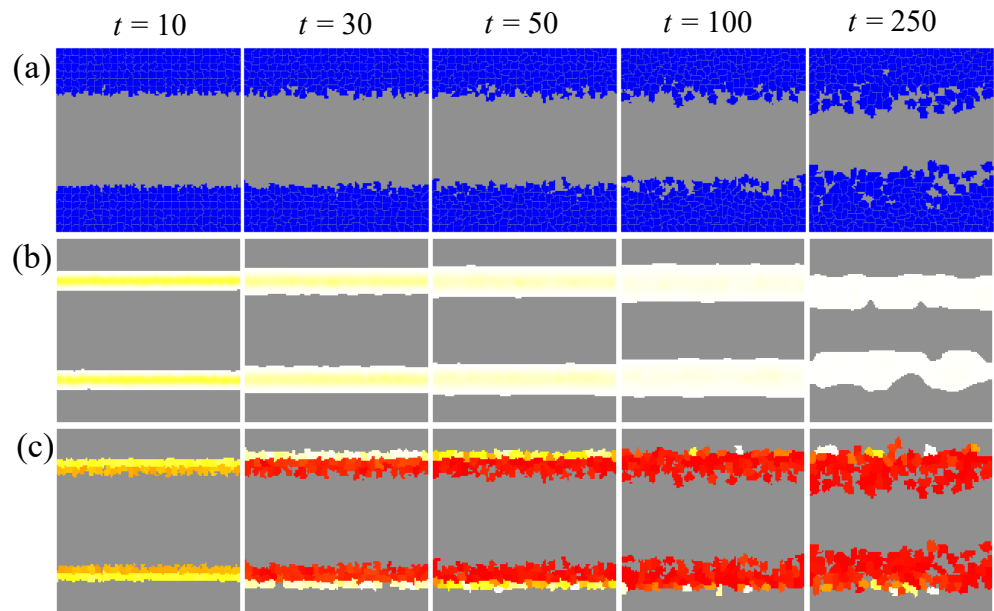


Figure 3. Time evolution of the distribution of cells (a), ATP (b) and Ca^{2+} (c) at the early stage. Red (white) indicates that the concentration of the chemical components is high (low), and gray indicates that the concentration of them is zero (almost zero). ATP diffusion and the subsequent Ca^{2+} influx occur quickly although the wound gap is barely closed.

3.3. Differences in the wound closure rate

In order to investigate the difference in the wound closure rate, we here show the degree of cell migration at various location within the cell cluster and the distribution of the cell size.

We first calculate the average cell position (perpendicular to the wound gap) at various location within the cell cluster, that is, cells in the row facing the wound gap (cluster F in Fig. 1(a)), cells located in the middle row within the cell cluster (cluster M in Fig. 1(a)) and cells located in the back row within the cell cluster (cluster B in Fig. 1(a)), respectively. Figure 4 (a), (b) and (c) show the time evolution of the average cell position for each cluster in two models. Time evolution of the average position for cluster F is quite similar to that of the surface coverage by cells (Fig. 2). It indicates that the cell migration of the leading cells directly reflects the wound closure rate. On the other hand, the average cell positions for clusters M and B in the two models show completely different behaviors. In the ATP model, cells for clusters M and B also migrate forward, whereas they remain almost the same positions in the ATP-free model. It shows that quick cell migration for cluster F due to the ATP release causes the subsequent cell migration for clusters M and B in the ATP model.

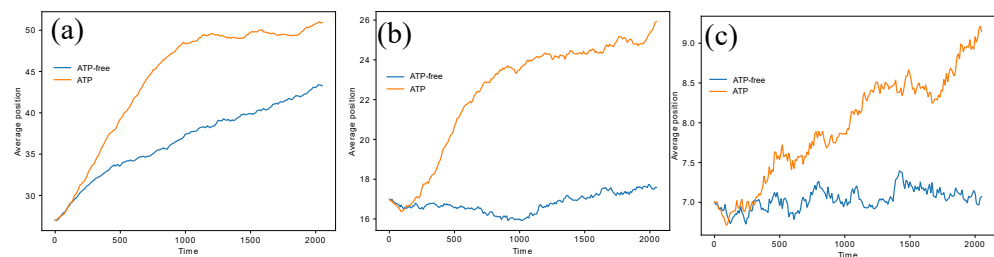


Figure 4. (a), (b) and (c) correspond to time evolution of the average cell position for clusters F, M and B, respectively.

We next visualize the distribution of the cell size for each cell cluster. Figure 5 (a) and (b) is basically the same as Figure 1 (b) and (c) but the color code is different: Differences in cell color indicate the differences in cell size. Blue color means the size of a cell is large ($V \simeq V_{\max}$), and white color means the size of a cell is small ($V \leq 25$). Figure 5 (a) clearly indicates that only the cells for cluster F grow and the size of the cells for cluster M and B (far from the wound) hardly changes in ATP-free model. To investigate it quantitatively, we calculate the average cell size at various locations for clusters F, M and B. Although cells for cluster F in two models have almost the same size over time (Fig. 6 (a)), cells at M and B in the ATP model grow faster than those in the ATP-free model (Fig. 6 (b) and (c)). This is the reason why the increase in the surface coverage slows down in the ATP-free model.

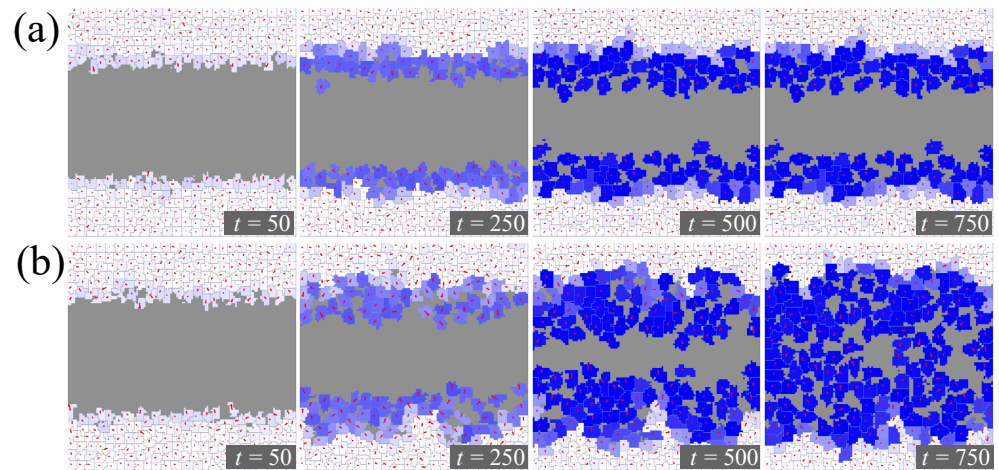


Figure 5. (a) and (b) correspond to Fig. 1 (a) and (b), respectively, and blue color indicates large cells whereas white color does small cells.

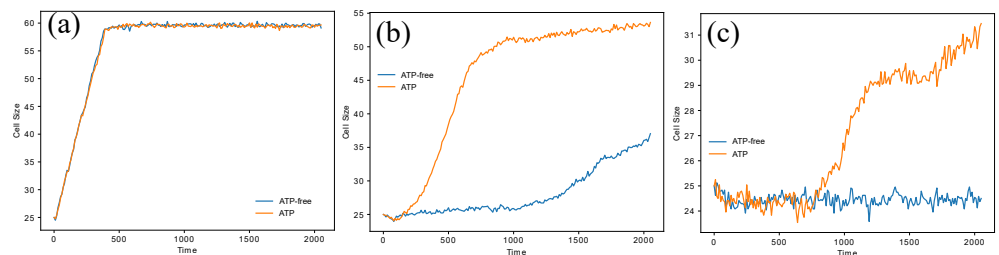


Figure 6. (a), (b) and (c) Time evolution of the average cell size for clusters F, M and B, respectively.

We next investigate why cells inside the cluster in the ATP-free model can hardly grow. In our numerical model, a cell surrounded by other cells cannot get large due to the contact inhibition. Therefore, vacant ratio of a cell, which denote how much space is available around the cell, is a useful for determining whether the cell can grow or not. Figure 7 (a), (b) and (c) show the time evolution of the average vacant ratio for clusters F, M and B, respectively. In ATP-free model, cells inside the cluster (clusters M and B) are almost completely surrounded by the other cells (average vacant ratio is almost zero), and thus they cannot get large due to the contact inhibition. Incidentally, the decrease in the vacant ratio for cluster F in the ATP model after $t = 700$ is due to the rapid migration and growing of the leading cells and the resulting loss of vacant space.

From the above considerations, we summarize the reason for the promotion of wound closure in the ATP model as follows. The cells inside the cluster also grow in the ATP model,

and rapid migration of cells on the surface makes space for the cells located away from the wound gap, resulting in the cell enlargement. Therefore, the collective cell migration induced by the ATP release and the Ca^{2+} influx promotes the cell growth inside the cell cluster and the consequent fast wound closure.

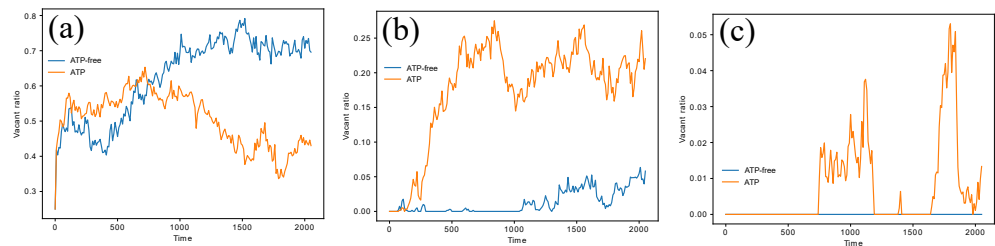


Figure 7. (a), (b) and (c) Time evolution of the average vacant ratio for clusters F, M and B, respectively.

4. Conclusions

We have introduced a hybrid model which consists of the CPM (cell dynamics) and the RD equations (dynamics for chemical components) for the wound closure process, and further added the cell polarity and contact inhibition. We here focused on the wound closure rate for the ATP-free model (without ATP release from the cells facing the wound) and the ATP model. The difference in the wound closure rate is caused by the rapid cell migration due to the ATP release and the subsequent Ca^{2+} influx induced by the mechanical forces, which we model as the polarity of the cell movement. The rapid cell migration makes space for the cells inside the cell cluster, and consequently causes rapid growth for these cells. On the other hand, in the ATP-free model, the leading cells migrate slowly, and thus the cells inside the cluster do not have enough space to get large and cannot grow due to the contact inhibition.

Our hybrid model can also be applied to the vascular network formation, where anisotropic shape of a cell is important to generate such a fibrous form. By incorporating the effect of cell shape and taking into account the effect of the ATP release induced by external forces, our hybrid model will be further extended to deal with the vascular network formation under mechanobiological conditions.

Author Contributions: Conceptualization, K.O., H.F.; methodology, K.O., H.F., H.T., R.O.; validation, K.O., H.F., H.T., R.O.; investigation, K.O., H.F.; data creation, K.O.; writing—original draft preparation, K.O.; writing—review and editing, K.O., H.F., H.T., R.O. All authors have read and agreed to the published version of the manuscript.

Funding: This research was partially supported by the Japan Society for the Promotion of Science (KAKEN 22K11941 to H.F., K.O., 19K12207 to K.O., H.F., H.T.) and AMED-CREST, AMED (JP20gm0810012) to K.O., H.F., H.T., R.O.

Institutional Review Board Statement: Not applicable

Informed Consent Statement: Not applicable

Data Availability Statement: Not applicable

Acknowledgments: We are grateful to Kazue Kudo, Yoshitaro Tanaka, and Shigeyuki Komura for inspiring and useful discussions.

Conflicts of Interest: The authors declare no conflict of interest.

Abbreviations

The following abbreviations are used in this manuscript:

CPM	Cellular Potts model
RD	Reaction-Diffusion (equations)
MCS	Monte Carlo step
ATP	adenosine triphosphate

References

1. Christopher R. Jacobs, Hayden Huang, Ronald Y. Kwon, *Introduction to Cell Mechanics and Mechanobiology*, Garland Science (2012).
2. Suvranu De, Wonmuk Hwang, Ellen Kuhl (editors), *Multiscale Modeling in Biomechanics and Mechanobiology*, Springer (2014).
3. Simon C. F. Rawlinson (editor), *Mechanobiology: Exploitation for Medical Benefit*, Wiley-Blackwell (2017).
4. Hayakawa, K.; Tatsumi, H.; Sokabe, M. Actin stress fibers transmit and focus force to activate mechanosensitive channels. *J. Cell Sci.* **2008**, *121*(4), 496–503.
5. Ingber, D. E. Tensegrity-based mechanosensing from macro to micro. *Prog. Biophys. Mol. Biol.* **2008**, *97*(2-3), 163–179.
6. Jansen, K. A.; Donato, D. M.; Balcioglu, H. E.; Schmidt, T.; Danen, E. H. J.; Koenderink, G. H. A guide to mechanobiology: Where biology and physics meet. *Biochim. Biophys. Acta.* **2015**, *1853*(11 Pt B), 3043–3052.
7. Ladoux, B.; Mege, R. Mechanobiology of collective cell behaviours. *Nat. Rev. Mol. Cell Biol.* **2017**, *18*(12), 743–757.
8. Huang, G. Mechanobiology in wound healing. *Biophys. J.* **2022**, *121*(2), 173–174.
9. He, S.; Li, X.; Ji, B. Mechanical force drives the polarization and orientation of cells. *Acta Mech. Sin.* **2019**, *35*(2), 275–288.
10. Thompson, W. R.; Scott, A.; Loghmani, M. T.; Ward, S. R.; Warden, S. J. Understanding Mechanobiology: Physical Therapists as a Force in Mechanotherapy and Musculoskeletal Regenerative Rehabilitation. *Phys Ther.* **2016**, *96*(4), 560–569.
11. Akaishi, S.; Akimoto, M.; Ogawa, R.; Hyakusoku, H. The relationship between keloid growth pattern and stretching tension: visual analysis using the finite element method. *Ann. Plast. Surg.* **2008**, *60*(4), 445–451.
12. Huang, C.; Holfeld, J.; Schaden, W.; Orgill, D.; Ogawa, R. Mechanotherapy: revisiting physical therapy and recruiting mechanobiology for a new era in medicine. *Trends Mol. Med.* **2013**, *19*(9), 555–564.
13. Huang, C.; Du, Y.; Ogawa, R. Mechanobiology and Mechanotherapy for Cutaneous Wound-Healing: Exploitation for Medical Benefit. In *Mechanobiology: Exploitation for Medical Benefit*; Rawlinson, S.C.F.; Wiley: 2016; pp. 239–253.
14. Fu, S.; Panayi, A.; Fan, J.; Mayer, H. F.; Daya, M.; Khouri, R. K.; Gurtner, G. C.; Ogawa, R.; Orgill, D. P. Mechanotransduction in Wound Healing: From the Cellular and Molecular Level to the Clinic. *Adv. Skin Wound Care* **2021**, *34*(2), 67–74.
15. Takada, H.; Furuya, K.; Sokabe, M. Mechanosensitive ATP release from hemichannels and Ca²⁺ influx through TRPC6 accelerate wound closure in keratinocytes. *J. Cell Science* **2014**, *127*, 4159–4171.
16. Graner, F.; Glazier, J. A. Simulation of biological cell sorting using a two-dimensional extended Potts model. *Phys. Rev. Letter* **1992**, *69*, 2128–2154.
17. Glazier, J. A.; Graner, F. Simulation of the differential adhesion driven rearrangement of biological cells. *Phys. Rev. E* **1993**, *47*, 2128–2154.
18. Merks, R. M. H.; Glazier, J.A. A cell-centered approach to developmental biology. *Physica A* **2005**, *352*, 113–130.
19. Hirashima, T.; Hosokawa, Y.; Iino, T.; Nagayama, M. On fundamental cellular processes for emergence of collective epithelial movement. *Biol. Open* **2013**, *2*(7), 660–666.
20. Guisoni, N.; Mazzitello, K. I.; Diambra, L. Modeling Active Cell Movement With the Potts Model. *Front. Phys.* **2018**, *6*, 61.
21. Czirók, A.; Varga, K.; Méhes, E.; Szabó, A. Collective cell streams in epithelial monolayers depend on cell adhesion. *New J. Phys.* **2013**, *15*, 075006.
22. Rens, E. G.; Edelstein-Keshet, L. From energy to cellular forces in the Cellular Potts Model: An algorithmic approach. *PLoS Comp. Biology* **2019**, *15*(12), e1007459.
23. Kapral, R.; Showalter, K. *Chemical Waves and Patterns*; Kluwer: Dordrecht (1995).
24. Kuramoto, Y. *Chemical Oscillations, Waves, and Turbulence*; Springer-Verlag: Berlin (1984) (Dover Edition, 2003).
25. Palachanis, D.; Szabó, A.; Merks, R. M. H. Particle-based simulation of ellipse-shaped particle aggregation as a model for vascular network formation. *Comp. Part. Mech.* **2015**, *2*, 371–379.
26. Suzuki, T. *Mathematical methods for cancer evolution*; Springer: (2017).
27. Barton, D. L.; Henkes, S.; Weijer, C. J.; Sknepnek, R. Active Vertex Model for cell-resolution description of epithelial tissue mechanics. *PLoS Comput. Biol.* **2017**, *13*(6), e1005569.
28. Ishihara, S.; Marcq, P.; Sugimura, K. From cells to tissue: A continuum model of epithelial mechanics. *Phys. Rev. E* **2017**, *96*, 022418.
29. Méhes, E.; Vicsek, T. Collective motion of cells: from experiments to models. *Integr. Biol.* **2014**, *6*, 831.
30. Szabó, A.; Unnep, R.; Méhes, E.; Tsal, W. O.; Argraves, W. S.; Cao, Y.; Czirók, A. Collective cell motion in endothelial monolayers. *Phys. Biology* **2010**, *7*, 046007.
31. Szabó, A.; Czirók, A. Individual Cell-Based Model for In-Vitro Mesothelial Invasion of Ovarian Cancer. *Math. Model. Nat. Phenom.* **2010**, *5*(12), 106–122.

32. Stott, E. L.; Britton, N. F.; Glazier, J. A.; Zajac, M. Stochastic simulation of benign avascular tumour growth using the Potts model. *Math. Comput. Model* **1999**, *30*, 183–198.
33. Szabó, A.; Merks, R. M. H. Cellular Potts modeling of tumor growth, tumor invasion, and tumor evolution. *frontiers in Oncology* **2013**, *3*, 97.
34. Odagiri, K.; Fujisaki, H. Mathematical Model for Wound Healing Caused by Exogeneous Mechanical Forces. *AIP Conference Proceedings* **2021**, *2343*, 020017.